Pure & Appl. Chem., Vol.55, No.5, pp.873-892, 1983.
Printed in Great Britain.

0033-4545/83/050873-20$03.00/0
Pergamon Press Ltd.

STRUCTURAL CHARACTERIZATION OF LINEAR POLYETHYLENE BY INFRARED SPECTROSCOPY

A. R. Wedgewood and J. C. Seferis

Polymeric Composites Laboratory, Department of Chemical Engineering, University of Washington, Seattle, Washington

Abstract - The structural features exhibited by a series of unoriented and uniaxially oriented linear polyethylene samples prepared under carefully controlled conditions have been examined by polarized and nonpolarized infrared experiments. Specifically, structural arrangements associated with the noncrystalline phase of the polymer have been examined both experimentally and theoretically. Experimentally, it was observed that the conformational arrangement of the noncrystalline phase was insensitive to density for samples whose bulk density was less than 0.96 g/cm^3. Above this value, significant conformational changes were observed with increasing density. Conformational changes with orientation were also analyzed theoretically by approximating the noncrystalline phase as a random coil. Comparisons of the experimental results with those predicted by the random coil model led to gauche (g) trans (t) conformational sequences to be assigned to the bands in the controversial 1200-1400 cm^{-1} region. Finally, quantitative measures of the crystalline and noncrystalline phase orientation functions were obtained from dichroic ratio measurements. Favorable comparison of the noncrystalline orientation values determined from the bands investigated in this work and the theoretical results of Flory and Abe and Nagai provide further support for the band assignments that are adopted here.

INTRODUCTION

Quantitative processing-structure-property relations are beginning to occupy a central role in the development of polymer science and engineering that one may safely draw an analogy to the metallurgical developments of the early years. Specifically, if crystalline polymers are considered as heterogeneous and anisotropic systems which offer tremendous potential for load bearing structural applications, the analogy is striking. However, when considering crystalline polymers both in processing and property modelling, as well as structure identification studies, care must be exercised that the noncrystalline phase is properly accounted for as an integral part of the material (1). Indeed, it has been well established that anisotropy and other morphological features are present in the noncrystalline phase and may control the exhibited bulk property behavior (2). However, unlike the crystal morphology and structure which may be identified with direct experiments (e.g., x-ray), the noncrystalline structure is only indirectly accessible and its quantitative description is very much model dependent. Thus, careful sample preparation under controlled processing conditions and simple experiments capable of characterizing morphology must be included in any program that attempts to develop processing-structure-property relations (3). Previous studies with polypropylene have demonstrated this point (2). Thus, when our studies were extended to polyethylene a well characterized sample base of films processed on experimental film lines was developed (4). Infrared spectroscopy was chosen as a key structure identification experiment since several studies have demonstrated that a variety of quantitative morphological information may be obtained. These include the percent crystallinity (5,6), the extent of chain branching (7,8) the second moment of the orientation of the crystalline and noncrystalline chain elements (9,10), and the conformation of the noncrystalline chain elements (11). Working with our carefully prepared samples, several new features have emerged from the infrared studies that are reported here and have also proved quite unique in further developments of constitutive structure-property relations (4).

EXPERIMENTAL

Eleven unoriented and five oriented linear polyethylene samples, which are briefly described in Tables 1 and 2, were investigated. All of these samples are linear polyethylenes, having less than 2 branches per 1000 carbons. Further structural, processing and property details concerning these samples can be found elsewhere (8). Assuming a two phase model, the weight fraction crystallinity was calculated with the following relation:

$$W_c = \frac{d-d_a}{d_c-d_a}\frac{d_c}{d} \quad (1)$$

where d_c and d_a are the crystalline and noncrystalline phase densities, respectively. Values of d_c = 1.00 (12) and d_a = 0.855 g/cm^3 (13) were assumed in this work.

TABLE 1. Specific extinction coefficient [cm^2/g] for the unoriented polyethylene samples

		Baseline #4					
Sample	W_c	e_{1078}	e_{1303}	e_{1352}	e_{1368}	e_{1894}	e_{2016}
Marlex A1	0.849	1.49	5.19	8.96	11.36	5.87	6.90
Marlex A2	0.881	1.32	3.99	7.09	8.56	5.98	7.11
Marlex A3	0.903	0.98	3.63	6.62	8.24	6.25	7.42
Marlex A4	0.841	1.45	4.48	7.91	10.18	5.92	6.74
A1-7840-A3	0.818	1.75	5.49	9.60	12.23	5.85	6.72
HU-10	0.742	2.53	8.64	12.75	16.78	5.17	6.15
HU-7	0.730	2.27	8.88	13.76	17.80	5.21	6.02
HU-5	0.691	2.97	10.81	17.10	22.26	4.75	5.91
HU-4	0.661	3.01	11.53	17.71	23.66	4.77	5.72
A1-7320	0.634	3.18	12.34	18.97	23.90	4.30	5.61
HU-3	0.588	3.30	13.35	20.59	26.91	4.11	5.36

TABLE 2. Dichroic Ratios and Specific Extinction Coefficients (cm^2/g) Measured for the Oriented Polyethylene Films

		Dichroic Ratios					
Sample	W_c	D_{1078}	D_{1303}	D_{1352}	D_{1368}	D_{1894}	D_{2016}
H-1	0.663	0.820	1.077	1.098	1.214	0.287	5.1
H-2	0.676	0.784	1.084	1.17	1.276	0.124	10.2
H-3	0.690	0.756	1.110	1.20	1.30	0.092	13.0
H-4	0.697	0.716	1.110	1.26	1.345	0.047	19.6
H-5	0.704	0.701	1.120	1.29	1.363	0.040	21.1

	Averaged Specific Extinction Coefficients					
Sample	e_{1078}	e_{1303}	e_{1352}	e_{1368}	e_{1894}	e_{2016}
H-1	2.69	8.89	13.37	21.14	4.65	5.97
H-2	2.53	8.88	13.08	20.58	4.74	6.1
H-3	2.37	8.21	12.43	19.61	4.95	6.25
H-4	2.30	8.13	12.00	19.50	5.05	6.31
H-5	2.26	7.72	11.44	18.43	5.10	6.32

Polarized and nonpolarized infrared measurements were made using a Nicolet 7199 FTIR spectrometer fitted with a Harric germanium polarizer and a Perkin-Elmer 283 spectrometer. The polarized measurements of the absorbance spectra were made with the incident radiation polarized parallel and perpendicular to the draw direction. The absorbance, A, was determined from these spectra using the peak height from baseline technique. This technique is suitable for quantitative analysis when the appropriate baseline is applied (6). The Nicolet spectrometer provides the absorbance as a function of wavelength, allowing the absorbance to be determined directly from the recorder trace. In contrast, the Perkin-Elmer spectrometer provided a trace of the percent transmittance T x 100 ($T = I/I_o$) as a function of wavelength, where I_o and I are the incident and transmitted intensities, respectively. To allow for quantitative interpretation of these spectra, the percent transmittance was converted to absorbance using the following relation:

$$A = \log_{10}(I_o/I) \quad (2)$$

The appropriateness and shortcomings of applying this relation have been discussed

elsewhere (6,14-16). The specific extinction coefficient was then calculated from the measured absorbance, A, the sample density, d(g/cm^3), and the sample thickness, b(cm), using the following expression (6):

$$e = A/b\ d\ (cm^2/g) \qquad (3)$$

Six absorbance bands (see Fig. 1), whose assignments are listed in Table 3, were investigated. The assignments for the noncrystalline 1078 cm^{-1} band, the crystalline 1894 cm^{-1} band, and composite 2016 cm^{-1} band appear to be well established (17-19,21).

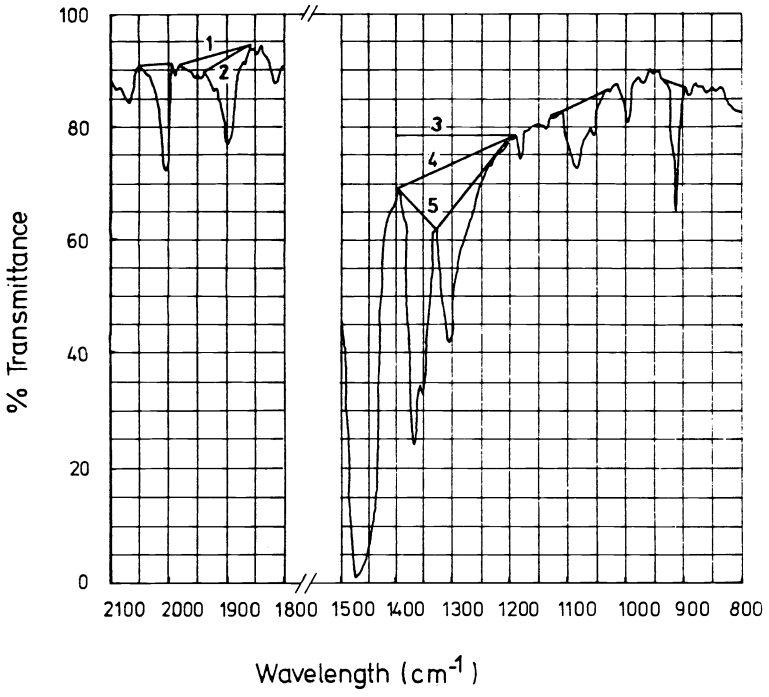

Fig. 1. Baselines for the evaluation of the polyethylene infrared spectra.

In contrast, the assignments of the noncrystalline 1303 cm^{-1} band and the doublet at 1352 and 1368 cm^{-1} have not been fully agreed upon (17-20). Based on the discussions of other investigators, the following assignments were adopted in this study: The 1303 cm^{-1} band was associated with a wagging of the CH_2 groups in the -gtg- and -gtg'- conformations (18). The assignments of Zerbi (20) were adopted for the 1352 and 1368 cm^{-1} bands, with the 1352 cm^{-1} band being attributed primarily to -gg- conformational pairs. The assignment of the 1368 cm^{-1} band to the -gttg- conformational sequence is consistent with the -tt- conformational assignment suggested by Neilsen and Holland (22), who studied the temperature dependence of this band. Further evidence supporting these assignments is provided in this study. However, experimental problems resulting from band overlap, especially in the 1320-1400 cm^{-1} range where as many as four absorption peaks have been proposed (8,18,23), makes explicit assignment of these absorption bands difficult.

The baselines used for evaluation of the 1078 and 2016 cm^{-1} bands are equivalent to the ones used in previous investigations of polyethylene (10,11,24). In contrast, the proper baselines for evaluating the 1303, 1352, 1368, and 1894 cm^{-1} bands, are ambiguous with, as is indicated in Figure 1, multiple baselines being proposed (6,11,25). In this study, the number 1 baseline was used to analyze the 1894 cm^{-1} band, while both the number 4 and 5 baselines were used to analyze the 1200-1400 cm^{-1} region. Okada and Mandelkern (6) also compared the results obtained using these baselines to analyze the 1200-1400 cm^{-1} region. They observed that, although the absolute values obtained were altered, the major trends were independent of the baseline used. To eliminate the errors caused by uncertainty of the proper baseline and band overlap, it is proposed that these bands be separated either graphically with a curve resolver or numerically using a computer program (26). When not otherwise specified, results for this region were obtained using the number 4 baseline.

TABLE 3. Assignments for the Polyethylene Absorption Bands

Band (cm^{-1})	Phase[a]	Transition Moment[b]	Conformation[c]	Assignment	References
1078	A	90	g and t	Skeletal C-C stretching mode.	17
			g	Intensity predominantly due to CH_2 wagging adjacent to gauche bonds.	18
1303	A	0	g	CH_2 twisting mode.	17,19
			gtg or gtg'	Antisymmetric CH_2 wagging mode.	18
					17
1352	A	0	g	CH_2 wagging	18
			gg	CH_2 wagging	20
			gg, gtg or gtg' and $(t)_n$-ggtgg-$(t)_m$	---	
1368	A	0	gtg or gtg'	Symmetric CH_2 wagging mode.	18
			gttg or gttg'	---	20,22
1894	C	90	tttt...	Combination of a Raman-active and IR active rocking mode.	17,19
2016	A + C	0	$\geq$ tttt	Combination of a Raman-active twisting mode and an IR active rocking mode.	10,17,21

(a) A - noncrystalline phase
C - crystalline phase

(b) angle between transition moment direction and the normal to the plane of the CH_2 group in degrees

(c) g - gauche conformation (+)
g'- gauche conformation (-)
t - trans conformation

THEORETICAL

Nonpolarized Measurements

In general, an absorbance at a particular wavelength may include contributions from chain segments in both the crystalline, A_c, and noncrystalline, A_a, phases. The absorbance associated with the chain segments in the noncrystalline phase, due to the conformational sensitivity of the infrared measurement, may be resolved into contributions from chain segments in either or both the gauche, A_{ag}, or trans, A_{at}, conformations. Furthermore, these components of the noncrystalline phase absorbance may depend on the sequential arrangement of these trans and gauche chain segments (see Table 3).

Attention is first given to the 1078 and 1894 cm^{-1} bands, which according to the assignments given in Table 3 are independent of the sequential arrangement of the chain segments. Treatment of the 1303, 1352, 1368, and 2016 cm^{-1} bands, which are dependent on the sequential ordering of the chain segment conformations, is then discussed.

To analyze the 1078 and 1894 cm^{-1} bands, the total absorbance at a given wavelength was assumed equal to the sum of the absorbances resulting from each contributing species at the same wavelength (14), viz:

$$A = A_c + A_a = A_c + A_{ag} + A_{at} \tag{4}$$

Using the Beer-Lambert law (14), the absorbance due to each contributing species, A_s, was then related to the sample thickness, b (cm), and the concentration of the absorbing species, C_s (g/cm^3). For example, the absorbance resulting from the crystalline material is given as:

$$A_c = e_c\, b\, C_c \tag{5}$$

where e_c is the crystalline extinction coefficient and C_c is the concentration of the absorbing crystalline chain segments. Defining similar expressions for the absorbances due to the noncrystalline chain segments in the gauche A_{ag} and trans A_{at} conformations and substituting these expressions along with equation (5) into equation (4) leads to the following expression for the specific extinction coefficient, viz:

$$e = \frac{A}{b\,d} = e_c \frac{C_c}{d} + e_{ag} \frac{C_{ag}}{d} + e_{at} \frac{C_{at}}{d} \tag{6}$$

In the above expression, e_{ag} and e_{at} are the extinction coefficients for the noncrystalline material in the gauche and trans conformations, respectively. The parameters C_{ag} and C_{at} are the concentrations of the noncrystalline material in the gauche and trans configurations contributing to the absorbance. Noting that the ratio of the concentration of a particular absorbing species and the material's density (C_s/d) is equal to the weight fraction of the absorbing species, W_s, equation (6) can be rewritten as:

$$e = e_c W_c + e_{ag} W_{ag} + e_{at} W_{at} \tag{7}$$

where W_c, W_{ag}, and W_{at} are the weight fractions of the respective absorbing species.

When one or more of the possible absorbing species does not contribute to the total absorption, its extinction coefficient is set equal to zero. For example, since the 1894 cm^{-1} absorption is due entirely to the crystalline chain segments, the extinction coefficient for this band is given as:

$$e_{1894} = e_{c_{1894}} W_c \tag{8}$$

where $e_{c_{1894}}$ is the extinction coefficient for a pure crystalline material, and the extinction coefficients for the noncrystalline material in the gauche and trans configurations have been set equal to zero.

The absorption at 1078 cm^{-1} has been attributed to the skeletal C-C stretching of noncrystalline chain segments in both the gauche and trans conformations (18). In view of this assignment, the specific extinction coefficient for this band may be defined as:

$$e_{1078} = e_{ag_{1078}} W_{ag} + e_{at_{1078}} W_{at} \tag{9}$$
$$= (e_{at_{1078}} + (e_{ag_{1078}} - e_{at_{1078}})q_g)W_a$$

where $e_{ag_{1078}}$ and $e_{at_{1078}}$ are the extinction coefficients for the noncrystalline chains in the gauche and trans conformations. The parameter q_g is the weight fraction of the noncrystalline chain segments in the gauche conformation (based on the total noncrystalline weight), and $W_a = 1 - W_c$ is the weight fraction of the noncrystalline chain segments (based on the total polymer weight), viz:

$$q_g = \frac{W_{ag}}{W_{ag} + W_{at}} = \frac{W_{ag}}{W_a} \tag{10}$$

The weight fraction of the noncrystalline chain segments in the gauche conformation, q_g, has been estimated to be on the order of .33-.5 for molten polyethylene (24,27,28). It has been experimentally estimated from x-ray scattering measurements to range between 0.35-0.4 for a typical polyethylene sample (29).

Although the 1078 cm^{-1} band is attributed to the C-C bond stretching in both the trans and gauche conformations, the transition dipole for the former is very small due to the centrosymmetry of this bond (18). Consequently, this absorption may be assumed to depend predominantly on the bonds in the gauche configuration (i.e., $e_{at1078} = 0$). Making this assumption, equation (9) becomes:

$$e_{1078} = e_{ag_{1078}} q_g W_a \tag{11}$$

implying that e_{1078} is directly proportional to the weight fraction of noncrystalline material in the gauche conformation.

Analysis of the 2016 cm^{-1} band is complicated by its dependence on both the noncrystalline material existing in sequences of four or more trans chain segments and the crystalline phase material. In view of the above assignment, the specific extinction coefficient was defined:

$$e_{2016} = e_{c_{2016}} W_c + e_{a\text{-}tttt_{2016}} q_{tttt} W_a \tag{12}$$

where q_{tttt} is the weight fraction of the noncrystalline material having four or more trans sequences in a row. The parameters $e_{c_{2016}}$ and $e_{a\text{-}tttt_{2016}}$ are the pure crystalline and pure noncrystalline phase extinction coefficients, respectively.

Analysis of the 1303, 1352, and 1368 cm^{-1} noncrystalline absorption bands is further complicated by their dependence on the sequential arrangement of the noncrystalline chain segments. As discussed earlier, the assignments for these bands are not fully agreed upon. In lieu of unequivocal assignments for these bands, the assignments given in the experimental section of this chapter are assumed in the following development.

Applying the procedure outlined above, the specific extinction coefficient for each of these bands can be expressed as:

$$e_{1303} = e_{a\text{-}gtg_{1303}} q_{gtg} W_a \tag{13a}$$

$$e_{1352} = e_{a\text{-}gg_{1352}} q_{gg} W_a \tag{13b}$$

$$e_{1368} = e_{a\text{-}gttg_{1368}} q_{gttg} W_a \tag{13c}$$

where q_{gtg}, q_{gg}, and q_{gttg} are the weight fractions of the noncrystalline chain segments in the designated conformational sequence. The extinction coefficients for these conformation sequences in the pure noncrystalline phase are appropriately defined for each of these absorbance bands (i.e., $e_{a\text{-}gtg_{1303}}$, $e_{a\text{-}gg_{1352}}$, and $e_{a\text{-}gttg_{1368}}$).

Because of the conformational dependence of these bands, their complete analysis requires that the weight fraction in each of these sequential arrangements be measured. However, in view of the fact that q_g can only be estimated, a determination of the amount of material in a given sequential arrangement cannot be made. Despite the uncertainty of q_g, q_{gg}, q_{gtg}, q_{gttg}, and q_{tttt}, which greatly hinders quantitative analysis of these bands, the relationships provided still remain as useful guides for interpretation of the infrared absorbance spectra. For example, a relative measure of the weight

fraction of noncrystalline material in a given conformational sequence may be obtained between any two samples using these relations. To illustrate, the relative weight fraction of chain segments contributing to the 1352 cm^{-1} band, relative to a reference sample (q_{gg}^{rel}), is defined here:

$$q_{gg}^{rel} = \frac{q_{gg}}{q_{gg}^{ref}} = \left[\frac{e_{1352}}{W_a}\right]\left[\frac{W_a}{e_{1352}}\right]^{ref} \tag{14a}$$

Using the appropriate expressions for the specific extinction coefficients, similar relations can be derived for the 1303 and 1368 cm^{-1} bands:

$$q_{gtg}^{rel} = \frac{q_{gtg}}{q_{gtg}^{ref}} = \left[\frac{e_{1303}}{W_a}\right]\left[\frac{W_a}{e_{1303}}\right]^{ref} \tag{14b}$$

$$q_{gtg}^{rel} = \frac{q_{gtg}}{q_{gtg}^{ref}} = \left[\frac{e_{1368}}{W_a}\right]\left[\frac{W_a}{e_{1368}}\right]^{ref} \tag{14c}$$

An important property of these expressions is that the calculated relative conformation ratios are independent of the noncrystalline density assumed for the calculation of W_a. This can be readily proved by showing that the ratio of the noncrystalline weight fractions calculated assuming two different noncrystalline phase densities is equal to a constant which is independent of the polymers bulk density. These relations are, however, dependent on the value assumed for the crystalline phase density, d_c, as are all the relative conformation ratios derived in this work.

Using equation (9), the following expression was obtained for the cm^{-1} band:

$$q_g^{rel} = \frac{q_g}{q_g^{rel}} = \frac{\left[\frac{e_{1078}}{W_a}\right] - e_{at_{1078}}}{\left[\frac{e_{1078}}{W_a}\right]^{ref} - e_{at_{1078}}} \tag{14d}$$

Unlike the previous results, this ratio depends on the magnitude of d_a. Furthermore, equation (14d) is only valid when $e_{at_{1078}}$ and $e_{ag_{1078}}$ are not equal.[a] If these extinction coefficients are equal, it can be readily shown that the 1078 cm^{-1} absorbance is independent of conformational changes. Recalling from Table 3 that this absorbance band arises predominantly from bonds in the gauche conformation (i.e. $e_{at_{1078}}=0$), equation (14d) can be rewritten as:

$$q_g^{rel} = \frac{q_g}{q_g^{ref}} = \left[\frac{e_{1078}}{W_a}\right]\left[\frac{W_a}{e_{1078}}\right]^{ref} \tag{14e}$$

Since this expression has the same form as equation (14a through 14c), q_g^{rel} calculated from it will also be independent of the noncrystalline density assumed. Noting that q_g^{rel} and $e_{at_{1078}}$ must be positive, the effect of using equation (14e) when $e_{at_{1078}}$ is not equal to zero can be readily obtained. A comparison of equation (14d) and (14e) shows that incorrectly assuming $e_{at_{1078}} = 0$, when $[e_{1078}/W_a] < [e_{1078}/W_a]^{ref}$ results in overestimating q_g^{rel}, while when $[e_{1078}/W_a] > [e_{1078}/W_a]^{ref}$ it results in underestimating q_g^{rel}. When these ratios are equal, $q_g^{rel} = 1$ independent of $e_{at_{1078}}$.

Applying the same procedure outlined above, the following expression can be obtained for the 2016 cm^{-1} band:

$$q_{tttt}^{rel} = \frac{q_{tttt}}{q_{tttt}^{ref}} = \left[\frac{e_{2016} - e_{c_{2016}} W_c}{W_a}\right]\left[\frac{W_a}{e_{2016} - e_{c_{2016}} W_c}\right]^{ref} \tag{14f}$$

The relative conformation calculated with this expression depends on both $e_{c_{2016}}$ and the value assumed for d_a.

The relative conformation ratios derived above allow for comparisons between the same absorption band in different samples. Other relations can also be developed to monitor

relative conformation changes between different bands measured for the same sample. For example, if the extinction coefficients are considered to be constants, the ratio of e_{1303} and e_{1352} is proportional to the relative amount of material contributing to these bands (i.e., q_{gtg}/q_{gg}), viz:

$$\frac{e_{1303}}{e_{1352}} = \frac{e_{a\text{-}gtg_{1303}}\, q_{gtg}}{e_{a\text{-}gg_{1352}}\, q_{gg}} \tag{15}$$

Similar expressions may be derived between any other two noncrystalline bands, using equations (11 through 13).

Polarized Measurements

To characterize the orientation of the polymer chains in the drawn samples, polarized infrared measurements were made with the radiation polarized parallel and perpendicular to the film draw direction. From these measurements the dichroic ratio, D, which has been defined (9,10) as:

$$D = e_{\parallel}/e_{\perp} \tag{16}$$

was calculated. For a uniaxially oriented film, the dichroic ratio and the Hermans' orientation function (26) for the chain segments contributing to the absorbance band analyzed are related (9,10) by:

$$f = \frac{D - 1}{D + 2}\,\frac{D_o + 2}{D_o - 1} \tag{17a}$$

where D_o is defined as

$$D_o = 2\cot^2 \Psi \tag{17b}$$

In the above relation, Ψ is the angle between the chain axis of the absorbing segment (the normal to the plane of the CH_2 group in the case of polyethylene) and the transition moment for the vibrational mode. Consequently, if Ψ is known, the average orientation of the chain segments contributing to the absorbance can be determined from the measured dichroic ratio. The values of Ψ reported by various investigators and used in this study are provided in Table 3. When interpreting the results calculated using these values, it must be kept in mind that the transition moment angles provided for the noncrystalline absorbance bands, especially those resulting from two or more CH_2 groups arranged in a specific conformational order, are only approximate.

For all but the 2016 cm^{-1} absorbance band, which contains contributions from both crystalline and noncrystalline chain segments, the dichroic ratio can be calculated directly from the measured specific extinction coefficients with equation (16). To analyze the 2016 cm^{-1} band, the crystalline and noncrystalline contributions were separated following the procedure outlined by Read and Stein (6). Their analysis of the dichroic ratio for the noncrystalline chain segments contributing to the 2016 cm^{-1} absorbance, when carried out on a weight fraction basis, yields the following expression:

$$D^a_{2016} = \frac{e_{2016_{\parallel}} - W_c\, e^o_{c_{2016}}(1 + 2 f_c)/3}{e_{2016_{\perp}} - W_c\, e^o_{c_{2016}}(1 - f_c)/3} \tag{18}$$

where $e^o_{c_{2016}}$ is the extinction coefficient for a perfectly oriented crystal with the radiation polarized along the c-axis of the crystal. This extinction coefficient, $e^o_{c_{2016}}$, can be determined from the extinction coefficient measured for a pure unoriented crystalline material, $e_{c_{2016}}$, viz:

$$e^o_{c_{2016}} = 3\, e_{c_{2016}} \tag{19}$$

For a uniaxially oriented sample the average specific extinction coefficient, e_{un}, which is proportional to the amount of absorbing species, can be defined as (9,10):

$$e_{un} = (e_{\parallel} + 2\, e_{\perp})/3 \tag{20}$$

By definition, e_{un} is equal to the specific extinction coefficient which would be measured for an unoriented sample having the same concentration of the absorbing species. Thus, measures of e_{un} can be used with the relative conformation ratio expressions to examine conformation changes in the noncrystalline phase with orientation.

Intermolecular and Intramolecular Interactions

The infrared spectra of most hydrocarbon polymers are adequately interpreted by neglecting intermolecular interactions and treating the polymer as an isolated chain (20,31,32). However, for simple polymers, such as polyethylene, intermolecular interactions in the crystalline lattice have been found to affect the infrared response (32,33). For example, intermolecular interactions in the polyethylene crystal unit in splitting both the methylene-scissoring ($\sim$1460 cm^{-1}) and the methylene-rocking ($\sim$725 cm^{-1}) bands (19,20,33). In these examples, the repetitive nature of the lattice enhances what would otherwise be weak intermolecular interactions. This enhancement effect is illustrated by the dependence of the 720 and 730 cm^{-1} extinction coefficients on the thickness of the crystal (34). Consequently, a three dimensional treatment, accounting for the intermolecular interactions, is needed to interpret the infrared response of the crystalline phase (33). Nonetheless, if the crystal type and size are not substantially changed with processing, one would expect the crystalline extinction coefficients and transition moments to remain approximately constant.

In contrast, for the disordered and loosely packed noncrystalline regions, intermolecular interactions are substantially reduced and thus may be neglected. Zerbi (20, 23), who also assumed negligible intermolecular interactions for hydrocarbon polymers, has provided additional evidence and discussion supporting this assumption. Since the intermolecular interactions in the highly ordered densely packed crystal lattice are weak, this assumption will most likely apply even in the case of moderately oriented noncrystalline regions.

It is well established in the literature that intramolecular forces are at least an order of magnitude greater than intermolecular forces (20). Consequently, in the absence of strong intermolecular interactions, such as hydrogen bonding, it is reasonable to assume that the infrared response of the noncrystalline region is dominated by the more pronounced intramolecular interactions. Snyder (18) and Zerbi (20) have shown that many of the noncrystalline bands arise from vibrational modes localized within specific conformational sequences. Since the infrared measurement is sensitive to the conformational arrangement of adjacent and neighboring chain segments, these intramolecular interactions are explicitly accounted for and segregated by the infrared measurement. Due to the large size of the polymer chain, intramolecular interactions between chain segments separated by many other chain segments are also possible. For all practical purposes, these interactions are similar to other intermolecular interactions and can be neglected. Therefore, it is assumed that the infrared response of the low and moderately oriented noncrystalline regions of polyethylene, depends only on the conformational arrangement of adjacent and near neighbor chain segments. This implies that for low to moderate orientations the noncrystalline extinction coefficients and transition moments may be treated to be approximately constant.

RESULTS AND DISCUSSION

Dependence on Crystallinity

To investigate the dependence of these absorption bands on crystallinity, the specific extinction coefficients were measured for the eleven unoriented samples described in Table 1. These values, which are also provided in Table 1, are plotted as a function of weight fraction crystallinity in Figs. 2 and 3. In accordance with equations (8,11-13), a linear regression analysis was performed for each of these bands. The best-fit lines, slopes, and intercepts obtained are provided in Figs. 2 and 3.

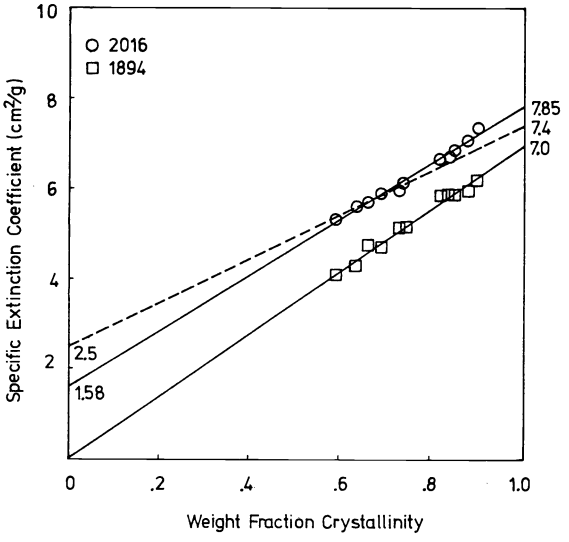

Fig. 2

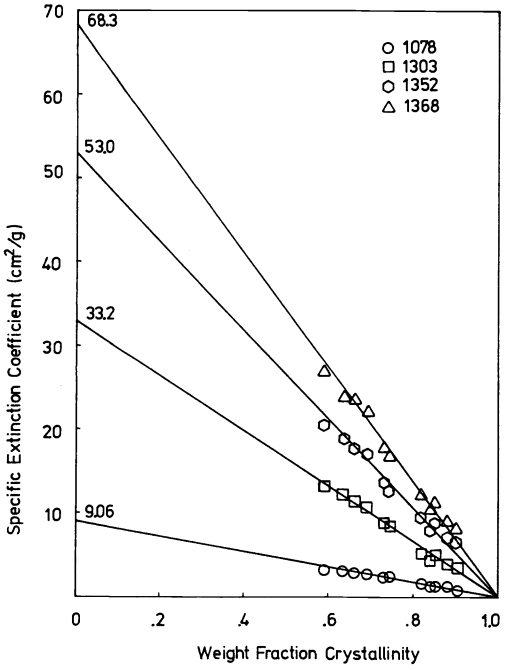

Fig. 3

Fig. 2. Specific extinction coefficient for the 1894 and 2016 cm^{-1} bands as a function of weight fraction crystallinity for unoriented linear polyethylene. Best fit lines, obtained with all and $d < 0.96$ g/cm^3 samples indicated by (——) and (— —), respectively, are provided for the 2016 cm^{-1} band.

Fig. 3. Specific extinction coefficient for the 1078, 1303, 1352, and 1368 cm^{-1} bands, determined using baseline 4, as a function of weight fraction crystallinity for linear polyethylene.

The linear dependence of the 1894 cm^{-1} crystalline band, indicates that the crystalline extinction coefficient, $e_{c_{1894}}$, for a pure crystalline material is constant over the crystallinity range investigated (see equation 8). The value obtained for this extinction coefficient, $e_{c_{1894}}$ =7.0 cm^2/g, is larger than the values reported by other investigators. This difference may be due to the use of different baselines. For example, Read and Stein (10) obtained a value of $e_{c_{1894}}$ =6.4 cm^2/g using baseline 2. A review of Figure 1 shows that the use of baseline 2 instead of baseline 1 would yield lower values.

Extrapolation of the data measured for the 2016 cm^{-1} band to $W_c = 0$ confirms the composite nature of this band. Although slightly lower, the values obtained for $e_{c_{2016}} = 7.85$ and $e_{a\text{-}tttt_{2016}} = 1.58$ cm^2/g are in good agreement with the results of Read and Stein (10). The linear dependence observed for this band implies that the difference, $e_{a\text{-}tttt_{2016}} q_{tttt} - e_{c_{2016}}$, is a constant independent of crystallinity (see equation 12). If these extinction coefficients are constants independent of morphology, this result implies that q_{tttt} is a constant independent of crystallinity. As will be shown later, based on the results observed for the noncrystalline bands, this conclusion is false.

The linear dependence observed for the noncrystalline bands (1078, 1303, 1352, and 1368 cm^{-1}), indicates that the product of the extinction coefficients and the weight fraction of noncrystalline material contributing to each band is constant over the crystallinity range investigated (see equations 11 through 13). If the extinction of these bands are independent of morphology, this implies that the weight fraction of the noncrystalline phase material contributing to each of these absorptions is independent of crystallinity. However, this conclusion is false, illustrating a deception caused by the method of data treatment.

To reveal this deception, these data were reanalyzed applying two different methods. First, following the work of Okada and Mandelkern (6), the three possible ratios of the 1303, 1352, and 1368 cm^{-1} bands were calculated. Second, the ratio of the specific extinction coefficient measured for each band and the noncrystalline phase weight fraction, W_a, was calculated (see equation 15). Besides the values obtained in this work, these ratios were also calculated from the data tabulated by Okada and Mandelkern (6), who used baseline 5 for their analysis.

As is shown in Fig. 4, the e_{1303}/e_{1352} and e_{1303}/e_{1368} ratios both decreased with increasing density, for samples having densities greater than 0.96 g/cm^3. Below this density, these ratios were observed to remain constant. In contrast, the e_{1352}/e_{1368} ratio was observed to slightly increase with increasing density. Although the trends observed are independent of the baseline used, the absolute values of these ratios were dependent on the method of analysis used. The slight differences observed between our values and those of Okada and Mandelkern for the e_{1303}/e_{1352} and e_{1352}/e_{1368}

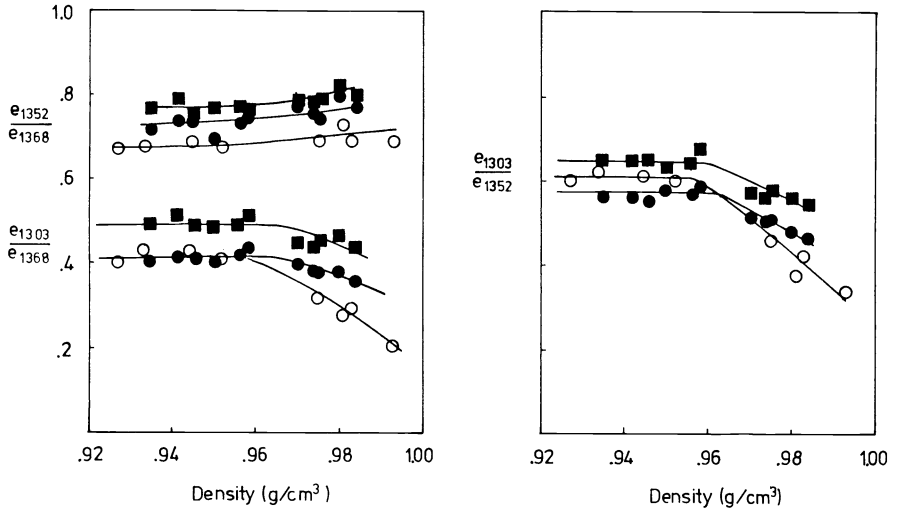

Fig. 4. Ratios of the 1303, 1352, and 1368 cm^{-1} specific extinction coefficients as a function of the bulk sample density. Solid symbols were obtained in this work, while open points are from Okada and Mandelkern (6). Circles and squares indicate data determined with baselines 4 and 5, respectively.

ratios may be indicative of morphological differences between the samples used in these studies. Direct comparisons of these data, however, must be made with caution, since these differences could also be due to instrument incompatibilities.

Since these are noncrystalline bands, the different absorption ratios observed for the high and low density samples must be attributed to differences in the interfacial and noncrystalline phase morphologies. Okada and Mandelkern (6), who observed the same trends with density, further related these differences to the crystallite morphology of the bulk crystallized samples. They argued that in the high density samples the crystallite thickness, $\langle l \rangle$, in the chain direction is comparable to the extended chain length, x, while for the low density samples the crystallite size is much smaller than the extended chain length. Calculating the interfacial free energy from the lamella thickness and the crystalline melting temperature, Mandelkern (35,36) showed that the interfacial free energy correlated with the ratio of the crystallite thickness and the extended chain length ($\langle l \rangle/x$). When this ratio approaches 1, as for the high density samples, the interfacial free energy was found to have its lowest value (2000 cal/mole), while when this ratio is very small as for the low density samples, the interfacial free energy becomes very large (8000 cal/mole). This large difference in the interfacial energies clearly indicates that different interfacial structures exist in the high and low density samples. However, as discussed by Mandelkern (35,36), the exact nature of these interfacial structures cannot be specified from this information alone.

In the case of the low density samples, $\langle l \rangle/x \ll 1.$, where it is geometrically possible to have a regular folded structure, it has been argued that the characteristic ratio, e_{1303}/e_{1352}, supports the existence of such an interfacial structure (6,35). Okada and Mandelkern (6) demonstrated that the value of this characteristic ratio, measured for the low density samples of 25°C, corresponded to the value obtained by extrapolation of

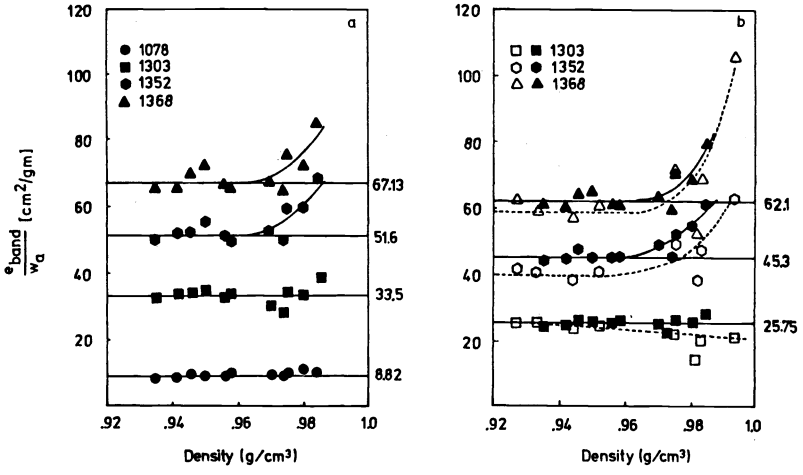

Fig. 5. Ratios of the 1078, 1303, 1352, and 1368 cm^{-1} specific extinction coefficients to the noncrystalline phase weight fraction as a function of the samples bulk density. Solid symbols were obtained in this work, while open symbols are from Okada and Mandelkern (6). The values in Figs. 5a and 5b were determined using baselines 4 and 5, respectively.

data measured for the pure melt of two n-paraffins. From this observation, they concluded that the bulk samples with densities less than 0.96 g/cm^3 have the same structure as the pure melt. They presented this conclusion as evidence that the postulation of a regular folded interfacial structure was untenable. Acceptance of this postulation, they argued, implied that the conformational arrangement in the pure melt for both the n-paraffins and the bulk crystallized polyethylene samples would have to be regularly folded. This observation, however, may be explained without excluding the existence of a regular folded structure. Since the fraction of the noncrystalline material in the interfacial region decreases with decreasing crystallinity (density), it can also be argued that contributions from the interfacial regions to these infrared bands are masked by the contributions from the bulk noncrystalline material. Consistent with this argument are the observations that the degree of crystallinity determined from density and infrared measurements are insensitive to the interfacial region. Therefore, one cannot ascertain that the agreement between the melt and bulk sample value of e_{1303}/e_{1352} precludes the existence of a regular folded interfacial structure.

For the high density samples, where the existence of a regular folded interface is geometrically precluded, due to the large $\langle l \rangle / x$ ratio (35,36), the observed changes in the extinction coefficient ratios may be explained by extending the same argument. As the sample's crystallinity increases, the proportion of noncrystalline material associated with the interfacial region increases, reaching a point where it begins to make a significant contribution to the absorbance spectrum. Therefore, changes in these extinction coefficient ratios may be a direct consequence of differences between the interfacial and bulk noncrystalline material. It may also be argued that the structural state of the bulk noncrystalline material changes with increasing crystallinity, due to the closely packed crystallites. Acting as barriers, these crystallites physically restrict the configurations that can be realized by the bulk noncrystalline material (37). For instance, as the spacing between crystallites becomes smaller, the noncrystalline chains will be forced to orient more and more parallel to the lamella surfaces. In view of the above discussion, one can only ascertain that the state of the noncrystalline material is being altered with increasing density. The precise region where this change occurs, however, cannot be unequivocally identified.

Close comparisons between our results and those of Okada and Mandelkern, show that the relative decrease of the e_{1303}/e_{1352} and e_{1303}/e_{1368} ratios for our samples is significantly less than the decrease they observed (6). This difference may be related to different sample preparation methods. The high density samples of Okada and Mandelkern were prepared by isothermal crystallization at 130°C for 40 days, while our high density samples were prepared by annealing at 130°C for a maximum of 180 hours (7.5 days) films that were initially cast and rapidly cooled from the melt. Based on the observations of Mandelkern et al. (38), who observed that the long period obtained by isothermal crystallization at a given temperature is larger than that obtained by prolonged annealing at the same temperature, it is expected that our samples are comprised of smaller crystals than the samples of Okada and Mandelkern (6,32). Furthermore, in the quenched samples, due to the rapid nucleation expected, many small spherulites are formed. Continued growth

of these spherulites upon annealing would be limited by interactions at these spherulite boundaries. In contrast, nucleation would be expected to be slower in the case of the isothermally crystallized samples, with fewer spherulites being formed. The growth of these spherulites will be less restricted by neighbor spherulites and thus would be expected to grow to much larger sizes than in the case of the quenched samples. Therefore, it is expected that the annealed samples used in this study consist of smaller spherulites, than those in the isothermally crystallized samples of Okada and Mandelkern. Although these expected structural differences may explain the differences observed between Okada and Mandelkern's and our samples, further investigation is needed to resolve the specific cause.

To identify changes in each of the individual absorbance bands, the ratio of the extinction coefficient and the noncrystalline phase weight fraction, W_a, were calculated and plotted as a function of density in Fig.5. As is shown, the ratios calculated for the 1352 and 1368 cm^{-1} bands are both observed to increase with density. Recalling the relative conformation expressions, developed as equations (14), this increase implies that the material contributing to these absorbance bands is increased with density.

The ratio for the 1303 cm^{-1} band remained nearly constant with density for our samples, while it decreased with increasing density for Okada and Mandelkern's samples (6). This result is surprising, in that it is not obvious why the conformational grouping contributing to this band (-gtg- and -gtg'- or -g-) would be decreased (or even remain constant), while the groupings contributing to the 1352 and 1368 cm^{-1} bands are increased. Furthermore, the different behavior observed for the 1303 and 1368 cm^{-1} bands strongly suggests that these bands are associated with material existing in different conformational sequences.

For the 1078 cm^{-1} band, this ratio appears to increase slightly with density. If $e_{ag_{1078}}$ is greater than $e_{at_{1078}}$, this would imply that the amount of gauche bonds is increased with sample density. This observation is consistent with the increase observed for the 1352 cm^{-1} band, which is associated predominantly with material in the -gg- conformational sequence. The opposite behavior observed for the 1303 cm^{-1} band suggests that assignment of the 1303 cm^{-1} band to the material in the -g- conformation is not correct and supports the -gtg- assignment adopted in this work (see Table 3). Based on the observations made above for these noncrystalline bands, a similar analysis of the composite 2016 cm^{-1} band was made. Since the conformational state of the noncrystalline samples with densities below 0.96 g/cm^3 was shown to be independent of density, the constants for the 2016 cm^{-1} band were redetermined using the six unoriented samples with $d < 0.96$ g/cm^3. The best fit line, slope, and intercept obtained by linear regression analysis of equation (12) are provided in Fig. 2. As is shown, these constants are significantly different from those obtained using all the samples.

Using the newly determined constant for $e_{c_{2016}}$ and the values provided for e_{2016} in Table 2, the product of $e_{a\text{-}tttt_{2016}}$ q_{tttt} was calculated from equation (12). This product is plotted as a function of density in Fig. 6. If it is assumed that $e_{a\text{-}tttt_{2016}}$ is a constant independent of density, the marked increase in this ratio implies that q_{tttt} increases with density. This observation is consistent with the argument of a barrier effect, supporting the postulation that the noncrystalline chains align parallel to the lamella surfaces (37). It is also consistent with the low interfacial free energy calculated by Mandelkern (35,36) for the high density samples.

Unlike the results obtained from the noncrystalline bands, this result was based on values extrapolated from only six unoriented samples which covered a narrow range of crystallinity. Errors due to this extrapolation may substantially alter the above result. Secondly, the crystalline extinction coefficient, $e_{c_{2016}}$, was assumed to be constant in this analysis. Although this appears reasonable in view of the behavior observed for the 1894 cm^{-1} crystalline band, it may not be valid. Changes in $e_{c_{2016}}$ with crystal size could alter this result.

Up to this point, the observed changes in the extinction coefficient ratios have been related to changes in the distribution of the gauche and trans conformations. These changes, however, could also be related to changes in the extinction coefficients with morphology. For instance, the intermolecular interactions near the interface could be substantially different from those in the bulk noncrystalline regions. Thus the extinction coefficient for a given conformational sequence may be different for material in the interfacial and bulk noncrystalline regions. However, it would be an unlikely

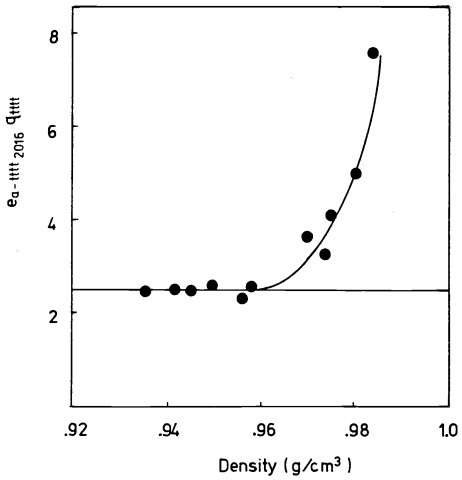

Fig. 6. The product of the noncrystalline extinction coefficient for the 2016 cm^{-1} band and the relative conformation ratio q_{tttt} as a function of the bulk sample density.

coincidence that the intermolecular interactions at the interface are altered to the extent that the extinction coefficients change, while the weight fraction of material contributing to the various conformational sequences remains unchanged. Consequently, we would still conclude from the above observations that the conformational state in the high density samples is different from that in the low density samples.

Conformation Changes with Orientation

The conformational state of the noncrystalline material and its changes with uniaxial orientation were investigated by analyzing the conformation sensitive 1078, 1303, 1352, 1368, and 2016 cm^{-1} bands. Changes in conformation with orientation were monitored, using the relative conformation ratios provided as equations 14. The reference properties required in these expressions were set equal to the properties of the unoriented low density ($d < 0.96$ g/cm^3) samples. Since the conformation state of these samples is constant and the density of the oriented samples is less than 0.96 g/cm^3, this reference state was the natural choice.

The reference properties were determined from these samples, using a linear regression analysis of equations (11 through 13). The reference properties obtained are provided for all but the 2016 cm^{-1} band in Fig. 5a. Values of $e_{c_{2016}} = 7.4$ and $e_{a-tttt_{2016}} q_{tttt} = 2.5$ cm^2/g, which were obtained for the 2016 cm^{-1} band, are provided in Fig. 2. Using these values along with the values for e_{un} (see equation 20) provided for the oriented samples in Table 2, the relative conformation ratios were determined. The results of these calculations are plotted as a function of draw ratio in Fig. 7. As can be seen, the relative weight fraction of material contributing to the 1303, 1352, and 1368 cm^{-1} bands was found to decrease with increasing draw ratio. The relative conformation ratio for the 1368 cm^{-1} band decreased the least of these three bands. The relative conformation for

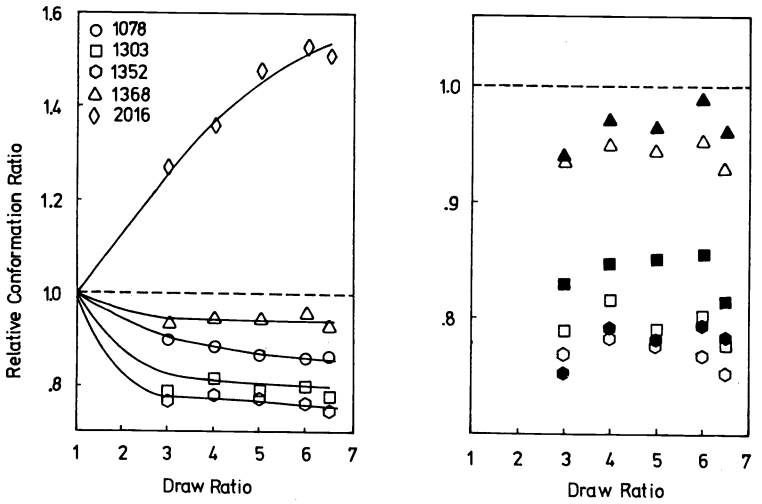

Fig. 7. Relative conformation ratio determined from the 1078, 1303, 1352, 1368, and 2016 cm^{-1} bands as a function of draw ratio. The open and solid symbols provided for the 1303, 1352, and 1368 cm^{-1} bands were determined using baselines 4 and 5, respectively.

the 1352 and 1303 cm^{-1} bands decreased the most, with the 1352 cm^{-1} band decreasing slightly more than the 1303 cm^{-1} band. The order in which these bands decreased agrees well with the data of Glenz and Peterlin (11), who investigated highly drawn polyethylene samples. Since each of these bands has been associated with at least one chain segment in the gauche conformation this result suggests that the fraction of the noncrystalline material in the gauche conformation is decreased with orientation.

These three bands were also analyzed using baseline 5, which yielded the reference properties given in Figure 5b. Using these values along with the e_{un} values determined for the oriented samples with this baseline, the above analysis was repeated. Although the relative conformation values calculated using baseline 5 were in almost all cases slightly larger, excellent agreement between the values calculated with these different baselines was found (see Fig. 7).

In contrast, the relative conformation ratio for the 2016 cm^{-1} band displayed a marked increase with draw ratio. Based on the assignment of this band, this observation indicates that the amount of noncrystalline material existing in long trans sequences is substantially increased with uniaxial drawing.

The values provided for the 1078 cm^{-1} band were calculated with equation (14e), which assumes $e_{at_{1078}}=0$. As shown in Fig. 7, the relative conformation ratio calculated making this assumption decreases with increasing draw ratio. Recalling that assuming $e_{at_{1078}}=0$ overestimates q_g^{rel} when $[e_{1078}/W_a] < [e_{1078}/W_a]^{ref}$, it was concluded that the amount of noncrystalline material in the gauche conformation is decreased with uniaxial stretching. Although this result contradicts the conclusion of Glenz and Peterlin (11), who found the 1078 cm^{-1} band insensitive to conformation changes, it is consistent with the assignment of Snyder (18).

A theoretical estimate of how these relative conformation ratios change with orientation was obtained by assuming that the noncrystalline material could be approximated as a random coil. The three-state random coil model for the polyethylene chain was assumed here (27,39). The statistical weight, σ, for a bond in the gauche conformation followed by a bond in the trans or gauche conformation of the same rotational sense, -tg- or -gg-, was assumed to be a variable dependent on the extent of orientation. The statistical weight, ε, of a gauche being followed by a gauche of the opposite rotational sense, -gg'-, was set equal to zero, eliminating the possibility of this arrangement.

The critical assumptions made in this theoretical treatment are: 1) intermolecular interactions in the noncrystalline phase are negligible and 2) the noncrystalline phase can be described using a single mean value for σ, even though it has a complex structure, consisting of loops, cilia, tie, and free chains. Since it is expected that the major proportion of the observed conformation changes occur in the orienting tie-molecules, the mean value of σ might have the following dependence of the weight fraction of taut tie-molecules, W_{tie}, (based on the total noncrystalline weight)

$$\sigma_{mean} = \sigma_{tie} W_{tie} + \sigma_{nc} (1 - W_{tie}) \qquad (21)$$

where σ_{tie} and σ_{nc} are the average statistical weights for the orienting tie-molecule and bulk noncrystalline material. As W_{tie} approaches zero, σ_{mean} approaches σ_{nc} and this model should describe the conformational state of the oriented noncrystalline material. Furthermore, when the conformational changes are small, this model may provide a reasonable description for the low density samples, which have conformation state similar to that of a pure melt (6,35). It may not be acceptable for the high density samples where the crystallites act as barriers, preventing many otherwise possible chain configurations.

Nagai (27) calculated the probability of occurrence for various conformational states, including -g-, -gg-, -gtg-, -gttg-, and -tttt-, as a function of σ. Assuming that the probability of occurrence is proportional to the weight fraction of a given conformational sequence, the relative conformation ratios with respect to a given reference state (see equations 14) were calculated from Nagai's results. Two different reference states, one corresponding to $q_g=0.33$ ($\sigma=0.3774$) and the other to $q_g=0.4$ ($\sigma=0.5439$), were used. In Fig. 8, the relative conformation ratios calculated assuming these reference states are plotted as a function of q_g^{rel}.

Assuming $e_{at_{1078}}=0$, q_g^{rel} was calculated from the 1078 cm^{-1} absorbance band. The relative conformation ratio calculated for the remaining absorbance bands are plotted as a function of q_g^{rel} in Fig. 8. As is shown, the 1352 cm^{-1} ratio was found to fall between the lines predicted for the -gtg and -gg- conformational sequences, supporting the assignments of Zerbi (20) and Snyder (18). The 1303 cm^{-1} ratio was found in the range predicted for the -gtg- sequence, supporting the assignment of Snyder (18),

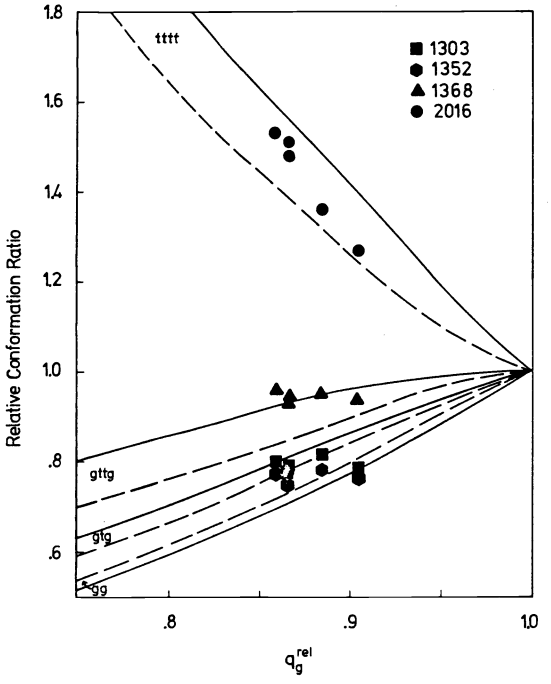

Fig. 8

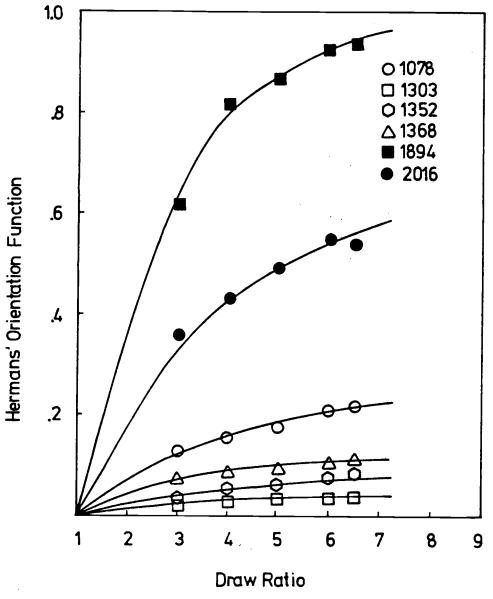

Fig. 9

Fig. 8. The relative conformation ratios determined for the 1303, 1352, 1368, and 2016 cm^{-1} bands as a function of the relative conformation ratio for the material in the gauche conformation, q_g^{rel}. Lines were calculated from the random-coil model (27,41) assuming $q_g = 0.33$ (— —) and $q_g = 0.40$ (——) in the unoriented reference state.

Fig. 9. Hermans' orientation function determined from the dichroic ratio measured for the different absorption bands examined as a function of draw ratio.

while the 1368 cm^{-1} ratio was found to be slightly above the values predicted for the -gttg- conformational sequence, supporting the assignment of Zerbi (20). The 2016 cm^{-1} ratio was found in good agreement with the values predicted for chain segments in sequences of four or more chain segments in the trans conformation, supporting its assignment (see Table 3). If $e_{at_{1078}}$ is not equal to zero, as was assumed, q_g^{rel} will been overestimated and the plotted results will all be shifted to lower values of q_g^{rel}. Although the agreement between the experimental and predicted relative conformation ratios is remarkable, it can not be considered conclusive evidence for the proposed band assignments. Representing the noncrystalline phase as a random coil for which only the statistical weight σ must be specified provides at best a crude approximation. Further investigations, using a more realistic model for the noncrystalline phase, are needed. Refinements of the simple model applied here, however, are not warranted, unless precise independent measures of q_g in the unoriented samples and d_a are obtained. Despite these uncertainties, the fact that the basic trends observed are consistent with those predicted by this simple model is satisfying. Furthermore, since intermolecular interactions are neglected by the random coil model, its apparent agreement with experimental data supports the assumption that intermolecular interactions in the noncrystalline regions are negligible.

In view of the above results, it was concluded that bonds in the gauche conformation are converted into trans conformation with uniaxial stretching. Adopting the assignment of Zerbi (20) for the 1368 cm^{-1} band, -gttg-, and that of Snyder (18) for the 1303 cm^{-1} band, -gtg-, it was concluded that the probability of finding a sequence of two or less bonds in the trans conformation was decreased. The marked increase observed for the 2016 cm^{-1} band indicates that the conversion of bonds in the gauche to trans conformation results primarily in the formation of extended chain segments.

Crystalline and Noncrystalline Phase Orientation

To analyze further the morphological arrangements of the oriented linear polyethylene samples, both the crystalline and noncrystalline phase orientation functions were determined from the polarized infrared measurements. The crystalline orientation function was determined from the 1894 cm^{-1} band, while the 1078, 1303, 1352, 1368, and 2016 cm^{-1} bands provided a number of measures for the noncrystalline orientation function. The values obtained from each of these bands are plotted in Fig. 9 as a function of draw

ratio. The different noncrystalline orientations measured from each band were attributed to the conformational sensitivity of these bands.

The orientation values obtained for the 2016 cm^{-1} band, f_a^{2016}, were calculated using equations 17 and 18, the dichroic ratios provided in Table 2, and a value of $e^o_{c_{2016}} = 22.2\ cm^2/g$. These values compare well with the values obtained by Read and Stein (10) and Miller and Jackson (40). The high orientation, relative to the orientations measured for the other noncrystalline bands, indicates that long trans sequences orient preferentially in the draw direction.

The orientation functions calculated for the remaining four noncrystalline bands were determined using the dichroic ratios provided in Table 2 and equations (16 and 17). Of these bands, the 1078 cm^{-1} band yielded the highest orientation, f_a^{1078}, falling between the values obtained for the 2016 cm^{-1} and the 1303, 1352, and 1368 cm^{-1} bands. Of the remaining three noncrystalline bands the 1368 cm^{-1} band yielded the highest orientation. The 1352 and 1303 cm^{-1} yielded the lowest orientations, with the 1352 cm^{-1} value being slightly larger than the 1303 cm^{-1} band. The dependence of these orientations on draw ratio are in good agreement with the results of Read and Stein (10).

From the orientation functions measured for these different infrared bands, the average noncrystalline phase orientation, f_a^{ir}, can be estimated using the following expression:

$$f_a^{ir} = f_{at} W_{at} + f_{ag} W_{ag} \tag{22}$$

where f_{at} and f_{ag} are the mean orientations of the noncrystalline material in the trans and gauche conformations. Recalling that the 1078 cm^{-1} band is due predominantly to bonds in the gauche conformation, f_{ag} was equated to f_a^{1078}. The weight fractions can be readily obtained from the reference and relative conformations, using $W_{ag} = 1 - W_{at} = q_g^{ref} q_g^{rel}$. Consequently, only f_{at} must now be specified, so that f_a^{ir} can be calculated.

Unfortunately, unlike f_{ag}, no single infrared band that gives a direct measure of f_{at} has been identified. However, information is available from the 2016 cm^{-1} band on the orientation, $f_{a>tttt} = f_a^{2016}$, and the amount of material existing in sequences of four or more bonds in the trans conformation, $W_{a>tttt} = q^{ref}_{tttt} q^{rel}_{tttt}$. Consequently, the contribution of the trans bonds to f_a^{ir} was split into two terms, a term for sequences of four or more bonds in the trans conformation and a term for sequences of three or less bonds in the trans conformation:

$$f_a^{ir} = f_{a_{<ttt}} W_{a_{<ttt}} + f_{a_{>tttt}} W_{a_{>tttt}} + f_{ag} W_{ag} \tag{23}$$

where the weight fraction of material in the <ttt sequences is given as $W_{a<ttt} = W_{at} - W_{a>tttt}$. Application of equation (23) to determine f_a^{ir} now only requires that $f_{a<tttt}$ be specified.

Although $f_{a<ttt}$ cannot be directly measured, it can be bounded between extremes that yield an upper and lower estimate for f_a^{ir}. To accomplish this bounding, the problem was formulated by setting:

$$f_{a_{<ttt}} = K f_{a_{>tttt}} \tag{24}$$

Thus, if K is specified, f_a^{ir} can be determined.

To obtain an estimate for K the theoretical results of Flory and Abe (41) and Nagai (27) for the three-state random coil model were employed. Applying these results to estimate K implicitly assumes that intermolecular interactions are negligible. The validity of this assumption has already been dicussed. The results of Flory and Abe (41) and Nagai (27) were expressed by Ward (42) as follows:

$$f_a = (G_2^*/2N)\ (V/V_o)^{2/3}\ (\lambda_e^2 - \lambda_e^{-1}) \tag{25}$$

where λ is the extension ratio, V is the sample volume in the strained state, V_o is the volume in a reference state, and N is the number of bonds. The parameter G_2^*, which was defined by Flory and Abe (41) provides a measure of the mean susceptibility of an axis to orient with respect to the end-to-end chain vector. In Nagai's formulation, $G_2^* = 2 f_k^*$, where f_k^* was defined to be the reduced orientation function (27). Values of G_2^* and f_k^* have been tabulated for various conformational sequences and transition moment directions (27,41). Flory and Abe (41) defined the local axes of the transition moments to conform to the symmetry of the various conformational sequences (see

Fig. 10), while Nagai (27) used the axis system depicted as Fig. 10c independent of conformational sequence. When using these different results, it is important to note that the orientation of the transition moment (a'), which was defined to be normal to the CH_2 plane, is twice the orientation of the transition moment (a), which was taken along the C-C bond (37).

Combining equations (24) and (25), the following expression for K in terms of G_2^* is easily obtained:

$$K^* = G_{2\,<ttt}^{\;*} / G_{2\,>tttt} \tag{26}$$

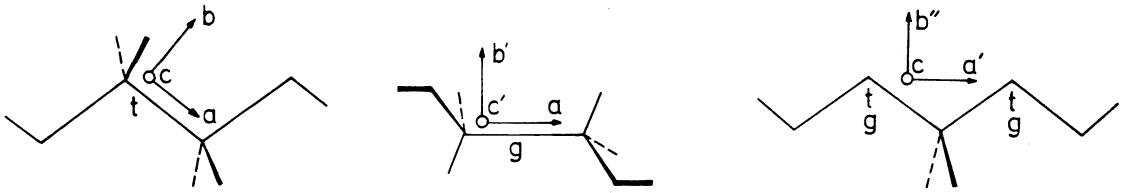

Fig. 10. Local orthogonal axes defined by Flory and Abe (41).

The parameter $G_{2\,>tttt}^*$ can be directly obtained from the results of Flory and Abe (41) and Nagai (27), while $G_{2\,<ttt}^*$ is given by:

$$W_{a\,<ttt}\; G_{2\,<ttt}^* = W_{at}\; G_{2\,t}^*\quad W_{a\,>tttt}\; G_{2\,>tttt}^* \tag{27}$$

where the parameter $G_{2\,t}^*$, which is for trans bonds with neighbors unspecified, has also been tabulated (27,41).

From the values of G_2^* tabulated for the a' axis, K was estimated to be between 0.25 and 0.55. Using these values for K, values of f_a^{ir} were calculated assuming reference states corresponding to both $q^{ref}_g = 0.33$ and 0.40. Since the assumption of these different reference states had little effect on the f_a^{ir} values calculated, only the average of these values is reported. As is shown in Fig. 11, the use of these different K values generated essentially the same values for f_a^{ir}. Thus, the values given in Table 4, which were generated assuming K = 0.4 are reported as the most probable values for f_a^{ir}. Also provided in Fig. 11 are the f_a^{ir} values calculated assuming K = 0 and 1. Since K = 1 implies that all the noncrystalline chains are fully extended and K = 0 implies that the sequences of <ttt are unoriented, these results represent conservative bounds for f_a^{ir}.

TABLE 4. Crystalline and Noncrystalline Orientation Functions

Sample	f_c	f_a^{ir}
H-1	0.625	0.17
H-2	0.825	0.21
H-3	0.870	0.24
H-4	0.930	0.28
H-5	0.940	0.28

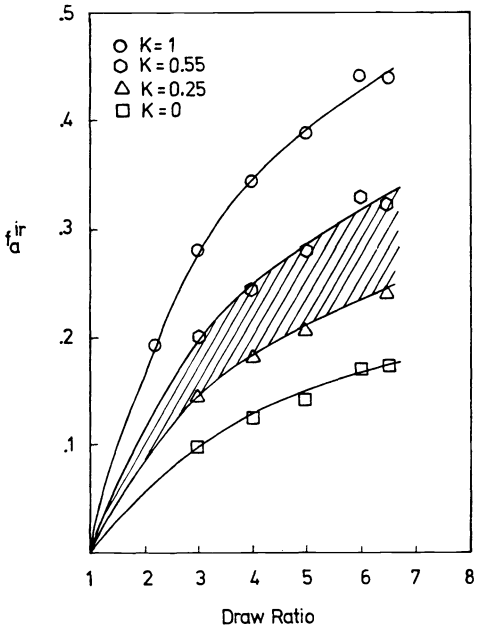

Fig. 11. The average noncrystalline orientation function as a function of draw ratio and the parameter K. Most probable range of values is indicated by the cross-hatched region.

To evaluate further the conformational assignments of the noncrystalline bands studied, an order of magnitude comparison between the orientations measured for each band and the theoretical G_2^* (or f_k^*) values (27,41) was made. Although only qualitative comparisons could be made, the theoretical G_2^* values were found to be consistent with the assignments adopted in this study.

CONCLUSIONS

The conformational arrangement of the noncrystalline material in bulk crystallized linear polyethylene was found to be independent of density, when $d < 0.96$ g/cm^3. Above this density, significant conformational changes were observed with increasing density. These changes were attributed to increased contributions from the interfacial regions and modifications of the bulk noncrystalline regions due to the barrier effect of the closely packed crystals.

Conformational changes with uniaxial orientation were monitored using the relative conformation ratios defined in this work. A theoretical interpretation of these changes was obtained by approximating the noncrystalline phase as a random coil. Comparisons of the experimental results with the predictions of this random coil model were found to be in good agreement, supporting the band assignments adopted here. In particular, evidence supporting the following assignments for the bands in the controversial 1200-1400 cm^{-1} region was provided: Assignments of the 1303 cm^{-1} band to the -gtg- or -gtg'-, the 1352 cm^{-1} predominantly to the -gg-, and the 1368 cm^{-1} band to the -gttg- or -gttg'- conformational sequences were supported. Furthermore, the remarkable agreement between the predictions of the random coil model and the observed behavior supports the assumption that intermolecular interactions in the noncrystalline regions are negligible.

Measures of the crystalline and noncrystalline phase orientation functions were obtained from the dichroic ratio measurements. From these orientation values, a single average orientation was obtained for the noncrystalline region. In addition, a comparison of the orientations determined for the different noncrystalline absorption bands investigated in this work with the theoretical results of Nagai (27) and Flory and Abe (41) was made. Qualitative agreement between their predicted and our experimental results further supported the band assignments adopted in this study.

Armed with the structural information provided in this study, constitutive relations for describing the bulk solid state properties of crystalline polymers such as dynamic mechanical, sonic modulus, and refractive index can now be developed on rational basis (4).

ACKNOWLEDGMENTS

Financial assistance for this work was provided by the National Science Foundation Polymers Program and Industry University Cooperative Program Grant #DMR-8113239. The H series polyethylene films were made in collaboration with Dr. R. J. Samuels while at Hercules, Inc., while the remainder sample data base was made by E. I. du Pont de Nemours & Co., under the supervision of Dr. G. Vassilatos. We are grateful to the above individuals and organizationa for their continuing interest and support of our work.

REFERENCES

1. J. C. Seferis and R. J. Gaylord, Eds., Polym. Eng. and Sci., 19 (1979).
2. J. C. Seferis and R. J. Samuels, Polym. Eng. and Sci., 19 975 (1979).
3. R. J. Samuels, "Structured Polymer Properties," John Wiley & Sons. Inc., New York (1974).
4. A. R. Wedgewood, "Quantitative Structure-Property Relations for Branched and Linear Polyethylene," Ph.D. Dissertation, University of Washington, Seattle, Washington (1982); A. R. Wedgewood and J. C. Seferis, in preparation.
5. H. Hendus and G. Schnell, Kunstoffe, 51, 69 (1961).
6. T. Okada and L. Mandelkern, J. Poly. Sci.: Pt. A-2, 5, 239 (1967).
7. J. Haslam, H. A. Willis, and D. C. M. Squirrell, "Identification and Analysis of Plastics," ILIFFE Books, London (1972).
8. D. R. Rueda, F. J. Balta Calleja, and A. Hidalgo, Spectrochimica Acta., 35, 847 (1979).
9. B. Jasse and J. L. Koenig, J. Macromol. Sci. Rev. Chem., C17, 61 (1979).
10 B. E. Read and R. S. Stein, Macromolecules, 1, 116 (1968).
11. W. Glenz and A. Peterlin, J. Macromol. Sci.-Phys., B4(3), 473 (1970).
12. C. W. Bunn, Trans Faraday Soc., 35, 482 (1939).
13. S. Matsuoka, J. Appl. Phys., 32, 2334 (1961).
14. K. Holland-Moritz and H. W. Siesler, Applied Spectroscopy Reviews, 11, 1 (1976).
15. D. A. Ramsay, J. Am. Chem. Soc., 74, 72 (1952).
16. R. Zbinden, "Infrared Spectroscopy of High Polymers," Academic Press, New York (1964).
17. S. Krimm, Advan. Polymer Sci., 2, 51 (1960).
18. R. G. Snyder, J. Chem. Phys., 47, 1316 (1967).
19. J. R. Nielsen and R. F. Holland, J. Mol. Spect., 6, 394 (1961).
20. G. Zerbi, Pure Appl. Chem., 26, 499 (1971).
21. J. R. Nielsen and A. H. Wollett, J. Chem. Phys., 26, 1391 (1957).
22. J. R. Nielsen and R. F. Holland, J. Mol. Spect., 4, 488 (1960).
23. D. R. Rueda, A. Hidalgo, and F. J. Balta Calleja, Spectrochimica Acta., 34, 475 (1978).
24. W. Glenz and A. Peterlin, J. Poly. Sci.: Pt. A-2, 9, 1191 (1971).
25. J. L. Koenig and D. E. Witenhafer, Macromol. Chem., 99, 193 (1966).
26. J. Pitha and R. N. Jones, Natl. Res. Council Canada Bull., 12, (1968).
27. K. Nagai, "Progress in Polymer Science Japan, Vol. 1" (edited by M. Imoto and S. Onogi), John Wiley & Sons, Inc., New York (1971).
28. R. Kitamaru and S. H. Hyon, J. Poly. Sci.: Macromolecular Review, 14. 207 (1979).
29. M. Numakawa and A. Odajima, Polymer J. (Japan), 13, 599 (1981).
30. P. H. Hermans, "Contributions to the Physics of Cellulose Fibers," Elsevier, New York (1946).
31. G. Zerbi, Applied Spectroscopy Reviews, Vol. II (edited by E. Brame), Marcel Dekker, Inc., New York (1969).
32. G. Zerbi and L. Piseri, J. Chem. Phys., 49, 3840 (1968).
33. M. Tasumi and T. Shimanouchi, J. Chem. Phys., 43, 1245 (1965).
34. D. R. Rueda, F. J. Balta-Calleja, and A. Hidalgo, J. Poly. Sci.: Phys. Ed., 15, 2027 (1977.
35. L. Mandelkern, Poly. Eng. and Sci., 6, 232 (1967).
36. L. Mandelkern. J. Poly. Sci.: Symposium, 43, 1 (1973).
37. V. Petraccone, I. C. Sanchez, and R. S. Stein, J. Poly. Sci.: Phys. Ed., 13, 1991 (1975).
38. P. H. Geil, "Polymer Single Crystals," John Wiley & Sons, Inc., New York (1963).
39. P. J. Flory, "Statistical Mechanics of Chain Molecules," John Wiley & Sons, Inc., New York (1969).
40. P. J. Miller and J. F. Jackson, ACS Polymer Preprints, 13, 335 (1972).
41. P. J. Flory and Y. Abe, Macromolecules, 2, 335 (1969).
42. I. M. Ward, "Structure and Properties of Oriented Polymers," John Wiley & Sons, Inc., New York (1975).